

Article

Optimization of Natural Circulation District Heating Reactor Primary Heat Exchangers

Jussi Saari , Heikki Suikkanen , Clara Mendoza-Martinez  and Juhani Hyvärinen

Department of Energy Technology, School of Energy Systems, Lappeenranta-Lahti University of Technology LUT, 53850 Lappeenranta, Finland

* Correspondence: saari@lut.fi

Abstract: Small modular reactors (SMRs) are gaining interest as a potential solution for cost-effective, carbon-neutral district heat (DH) production. The low pressures and temperatures permit much lighter and cheaper designs than in power plants, and efficiency is high as all heat generated can be sold to customers. In this work, the optimization of the primary heat exchangers in a natural-circulation 50-MW heating reactor concept was carried out to obtain an initial feasibility estimate for the concept for both baseload and load-following operation, as well as to obtain information on the characteristics of an optimized design. Studies on small natural circulation heat-only SMRs and the impact of heat exchanger design on the overall dimensions and economics have not been published before. Although a detailed heat exchanger cost model was used, the results should be considered tentative initial estimates, as much of the cost impact from the heat exchanger design comes from the effect the design has on the pressure vessel dimensions. While more detailed pressure vessel designs and cost functions are needed for final optimization, the feasibility of the concept is shown. Optimization for different load profiles produced near-identical designs, with the downcomer divided approximately in half between the heat exchanger at the top and an empty space at the bottom to maximize the pressure difference available for natural circulation. Although conservative, even pessimistic estimates were used in the absence of detailed cost functions, cost prices of 30–55 EUR/MWh_{DH} at a 10% interest rate were obtained, or only 20–40 EUR/MWh_{DH} at a 5% interest rate. This indicates potentially good competitiveness for the considered DH SMR concept.

Keywords: small modular reactors; district heating; shell-and-tube heat exchangers; optimization; cuckoo search



Citation: Saari, J.; Suikkanen, H.; Mendoza-Martinez, C.; Hyvärinen, J. Optimization of Natural Circulation District Heating Reactor Primary Heat Exchangers. *Energies* **2023**, *16*, 2739. <https://doi.org/10.3390/en16062739>

Academic Editors: Dan Gabriel Cacuci, Andrew Buchan, Michael M.R. Williams and Ruixian Fang

Received: 23 February 2023

Revised: 9 March 2023

Accepted: 12 March 2023

Published: 15 March 2023



Copyright: © 2023 by the authors. Licensee MDPI, Basel, Switzerland. This article is an open access article distributed under the terms and conditions of the Creative Commons Attribution (CC BY) license (<https://creativecommons.org/licenses/by/4.0/>).

1. Introduction

1.1. Background

Climate change is underway due to anthropogenic greenhouse gas emissions that are mainly caused by energy use: electricity, space heating in cold climates, and traffic fuels. In Finland, greenhouse gas emissions from power generation are already low, consistently below 70 kgCO₂/MWh [1], due to the large shares of nuclear, hydro, and biomass-based generation and the recently increasing amount of wind power. Space heating, however, is still 1/3 fossil-fueled [2]. District heating (DH) networks in the country are well developed, with a heating market share of 46% and the majority of the population within reach [2]. With a favorable public attitude toward nuclear energy [3], nuclear district heating is a potential solution for decarbonizing the remaining heating solution. In this work, the feasibility of a natural-circulation heat-only nuclear reactor is carried out by means of techno-economic optimization of the primary heat exchangers for such a concept.

1.2. District Heating Nuclear Reactors

A nuclear fission reactor liberates the nuclear binding energy of heavy elements. Macroscopically, nuclear energy manifests as heat released into the reactor fuel. Nuclear

energy is extremely resource efficient, making it ideal for energy system decarbonization and reduction of other environmental burdens associated with energy supply. Therefore, a nuclear reactor is an ideal source for heating applications, especially in societies where centralized heat supply (DH networks) already exists.

Nuclear reactors have been utilized for the cogeneration of electricity and DH with operating experience since the 1960s in the Swedish Ågesta heavy water reactor, which was used to provide heat to the Farsta borough of Stockholm [4]. In addition, IAEA [5] lists tens of reactors, especially in Russia, that have produced DH in addition to electricity. Using large conventional nuclear power plants for DH production is problematic, however, due to the conflicting requirements of needing distance from population centers for safety and proximity to heat consumers for economical heat delivery. Close-to-population siting is being explored for small modular reactors (SMRs), whose smaller size brings new possibilities to accomplish this safely.

The IAEA ARIS database on SMRs contains approximately 80 designs [6], most of which have been developed primarily for electricity production, with cogeneration or desalination options available in addition. Although considered in previous analyses for DH [7], small reactors with design choices dictated by the need to produce almost 300 °C steam for electricity production are economically sub-optimal for heat-only use, where only hot water at slightly over 100 °C is needed. Several low-temperature heat-only reactor designs have been developed in the past [8], such as the SECURE [9], considered but eventually not built for DH production in Finland in the 1970s. More recently, heating reactors have been developed in China, both in vessel and deep-pool configurations [10]. The main focus has been on the vessel-type NHR-200 for providing 200 MW_{th} of heat at up to 224 °C. Although a commercially-sized reactor has not yet materialized, an experimental NHR-5 reactor was completed in 1989 and has been operating successfully [11].

Considering that the existing commercial DH reactor designs, such as the NHR-200, are oversized for most DH networks outside the capital region in Finland and Scandinavia [12], decarbonizing heating by dedicated small heating reactors with thermal output in tens rather than hundreds of megawatts is a promising avenue for domestic technology development. LUT University [13] and VTT Technical Research Centre of Finland [14,15] have, therefore, embarked on concept designs of low-temperature, low-pressure, light-water moderated, and cooled heating reactors.

Being located at or near population centers, DH reactors need robust safety features. Together with the need for small unit size, this demands a design that is simple to construct and operate and that is reliant on physical mechanisms rather than complex system architectures for a high-safety level. High safety translates to confidence in the ability to mitigate all abnormal events and accidents so that emergency preparedness measures are not needed outside the plant fence.

Gravity never fails; natural convection and natural circulation are, thus, good choices for heat transfer from the reactor core to users in normal operation and to the environment in abnormal situations. In this paper, we focus on optimizing the heat exchangers for normal operation.

1.3. Heat Exchanger Optimization

The considered heat exchanger geometry is one of segmentally baffled shell-and-tube heat exchanger (STHE) placed vertically in the annular downcomer of the reactor, with the primary water flowing freely into and out from the tubes, without tube-side heads.

While techno-economic STHE optimization has been widely studied comparing a variety of metaheuristic optimizers for the purpose, the extensive literature is considered of little value for this work for two main reasons; firstly, the considered cost function is entirely different, and secondly, the inherent shortcomings of the simplistic area-based cost functions and focus on introducing new metaheuristics in almost all published studies. Earlier, it has been demonstrated that a simplified cost function alters the topography enough that the simple area-based cost correlations are unsuitable even for optimizer

performance evaluation or control parameter tuning [16]. Almost all the STHE optimization studies claim that the performances of their investigated metaheuristics are superior to other methods. The problems of STHE optimization studies are elaborated further in [17], and the problems of the metaheuristic field in general in [18,19].

In the absence of the reliable, relevant literature on problems similar to the one at hand, the optimizer choice was based on the authors' experiences. Differential evolution (DE) is a global optimizer proven to yield good performance in a variety of difficult multi-modal non-separable mixed-integer engineering problems ranging from wind farm optimization considering uncertainty [20] to a variety of heat exchanger design [16] and arrangement [21] problems. Recently, a new DE-based method, the cuckoo search (CS), has been applied to both heat exchanger [17] and wind farm [22] optimization, outperforming both other methods and the original DE itself. Based on this, the CS was selected for the task.

1.4. Goals

The main goal of this study was to obtain an initial estimate for the feasibility of a small natural circulation heating reactor design for baseload DH production in a large city as well as in a smaller DH network where much of the operation would be at partial loads. The results show that the impact of load profile assumption on the optimized heat exchanger configuration is negligible, and separate designs for constant baseload and varying-load uses are not needed. From the results of this study, information is also obtained on the broad outlines of likely optimal heat exchanger design features for such a reactor concept, an approximate cost price for the generated heat, and suitability and appropriate tuning parameters of the cuckoo search algorithm for the considered optimization task. Studies on small natural circulation heat-only SMRs and the impact of primary heat exchanger design on the overall dimensions and plant economic performance have not been published before.

2. Materials and Methods

2.1. District Heat Demand and Temperature Levels

The primary application for the considered reactor concept is providing district heating (DH) in a Nordic context. In Finland and Scandinavia, district heating dominates the urban heating markets. The implementation is almost always a two-pipe hot-water system, with supply and return temperatures typically varying between 70–120 °C, and 35–55 °C, respectively. The temperature levels vary seasonally and also between networks, depending on the climate and the types of heat consumers in the network.

The seasonal variation of the heat load is significant: in Finland, the winter peak consumption typically exceeds the summer minimum by a factor of ten. A discretized approximation of the annual temperature and load profiles is depicted in Figure 1 as duration curves. The DH load profile is based on [23]; ambient temperatures represent 10-year averages measured in Jyväskylä, a mid-size city in central Finland [24], and the DH supply temperature represents the recommended temperature curve as a function of ambient temperature in Finnish DH networks [25]. The return temperature represents average values measured in an operating network at a given supply temperature level [26].

Two scenarios are considered, baseload (BL) and mid-load (ML). In the BL scenario, the SMR operates at full thermal power (but varying temperature levels, Figure 1) for 8200 h annually. In the mid-load scenario ML, the DH SMR system is considered in a situation where the full load corresponds to 35% of the peak load of the DH system. Table 1 summarizes each load point with which the annual operating profile is approximated. The case BL was considered in two variants, the basic 50 MW and an additional 200-MW variant for a larger city. In the second case, BL200 four reactors are placed in line with a one-meter separation of containment vessels in an elongated rectangular pool cavity.

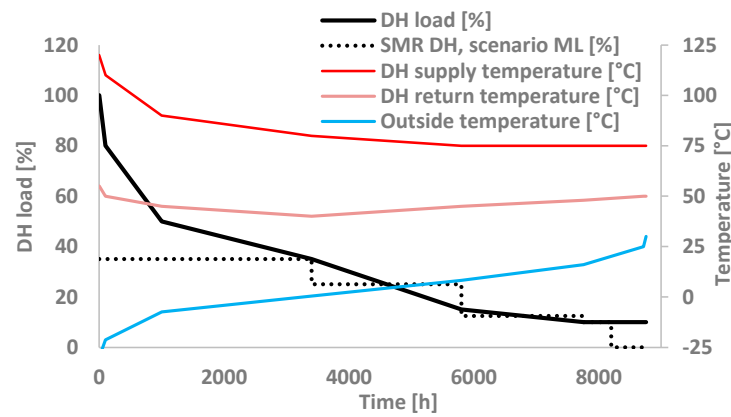


Figure 1. Duration curves of DH load (left axis), and DH water supply and return temperatures, and ambient temperature (right axis). The dotted line represents the discretized approximation for mid-load scenario ML.

Table 1. Discretized load profile approximation.

Load Point	t_{period} [h]	$F_{\text{DH, BL200}}$ [MW]	$F_{\text{DH, BL50}}$ [MW]	$F_{\text{DH, ML}}$ [MW]	T_{sup} [°C]	T_{ret} [°C]
1	100	200.0	50.00	50.00	120	55
2	900	200.0	50.00	50.00	100	48
3	2400	200.0	50.00	50.00	85	43
4	2400	200.0	50.00	35.71	78	40
5	1960	200.0	50.00	17.86	75	43
6	440	200.0	50.00	14.29	75	47
7	560	0	0	0	75	50

2.2. Studied District Heating SMR Concept

The considered pressurized water DH reactor is based on the design proposed in [14,15]. A notable feature is that the reactor pressure vessel (RPV) is enclosed inside another pressure vessel, the containment vessel (CV), placed in a water pool. Figure 2 depicts the schematic diagram of the considered SMR concept. An intermediate secondary circuit separates the reactor’s primary circuit from the DH network, connecting the two via heat exchangers. In the reactor pressure vessel, the heated primary circuit water flows up through the cylindrical riser, returning through the heat exchangers located in the annular downcomer. The primary circuit heat exchangers are 1:1 counterflow segmented-baffle shell-and-tube heat exchangers with the hot primary water in the tubes and secondary circuit water in the shell side. The construction is essentially one-pass welded TEMA E but without tube-side entry and exit headers.

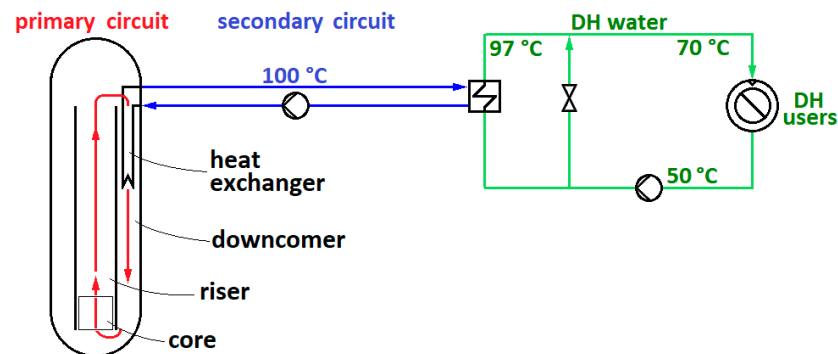


Figure 2. Schematic diagram of the considered district heating SMR concept. The temperatures do not correspond to any particular operating point or optimized design but indicate the typical warm-weather magnitudes and the purpose of the shunt connection.

The secondary circuit transfers heat to the DH network via plate heat exchangers. To lower the DH supply temperatures during warmer seasons while maintaining stable primary circuit conditions, a shunt connection, Figure 2, allows partial bypassing of the secondary heat exchangers.

2.3. Objective Function

The design of the heat exchanger affects not only the cost of the heat exchangers themselves but also the dimensions and, thereby, the cost of the reactor pressure vessel (RPV), containment vessel (CV), and, to some extent, the reactor pool. In the ML scenario, partial-load operation and full-load hours may also be affected. To consider these effects, annual net cash flow C_{net} maximization is considered as the objective function,

$$C_{\text{net}} = c_{\text{DH}}Q_{\text{DH}} - a C_{\text{TCI}} - c_{\text{el}}E_{\text{p}} - c_{\text{f}}Q_{\text{f}} - c_{\text{O\&M,var}}Q_{\text{DH}} - C_{\text{O\&M,fix}}, \quad (1)$$

where c_{DH} is the district heat (DH) price [€/MWh_{DH}], Q_{DH} is the annual DH production [MWh_{DH}], a [-] is the annuity factor to determine the annual amortization of the total capital investment C_{TCI} [€], c_{el} [€/MWh] is the purchased electricity price, E_{el} [MWh] is the pump electricity consumption to overcome the heat exchanged pressure drop, c_{f} [€/MWh] is the fuel price, Q_{f} [MWh_f] is the annual fuel use, and $c_{\text{O\&M,var}}$ [€/MWh_{DH}] and $C_{\text{O\&M,fix}}$ [€] are the variable and fixed operation and maintenance costs, respectively.

The assumed values of economic parameters are listed in Table 2, determining the pumping electricity consumption in Equation (1) is described in Section 2.4, and C_{TCI} is calculated by incrementing the base plant costs C_{SMR} with the free-on-board costs of the heat exchangers (HX), RPV, and CV, and the cost of the reactor pool cavity for the CV.

$$C_{\text{TCI}} = C_{\text{SMR}} + 3.3 (C_{\text{FOB,HX}} + C_{\text{FOB,RPV}} + C_{\text{FOB,CV}}) + C_{\text{cav}}, \quad (2)$$

where the factor 3.3 [27] is used to convert the free-on-board (FOB) costs of heat exchangers and pressure vessels to TCI costs. The reactor pool cavity cost C_{cav} represents the cost of excavating and building an extension downward from the 7-m-deep reactor pool (see Figure 3). The main pool is of fixed dimensions and cost, regardless of heat exchanger sizing, and is considered part of the C_{SMR} . The cavity dimensions are affected by the heat exchanger sizing, however, and, thus, are evaluated as a function of the resulting dimensions.

Table 2. Main cost data assumptions.

Property	Unit	Value
Economic lifetime	a	25
Interest rate	%	10
Specific total capital investment (TCI):	50 MW 4 × 50 MW	€ / kW _{th} 1866 ¹ 1233 ¹
District heat price	€/MWh _{DH}	70
Purchased electricity price	€/MWh _{el}	120
Nuclear fuel price	€/MWh _f	3.00
Operating and maintenance cost, variable	€/MWh _{th}	1.00 ²
Operating and maintenance cost, fixed	M €/a	1.50

¹ excluding the RPV and CV bare shell, reactor pool cavity, and the primary heat exchangers, ² excluding fuel cost, and the pumping power to overcome the heat exchanger pressure drop.

It should be noted that the C_{SMR} figure is tentative, based on the estimated cost of a reactor similar to the Chinese DHR-400 DH SMR built in Finnish conditions [28], scaled with a capacity scaling exponent of 0.7. Although this includes the RPV and heat exchangers, for a conservative estimate, the figure was not adjusted down. While the estimate has considerable uncertainty, as there are no small DH SMRs in Europe yet, other than the costs related to RPV, CV, and excavation, the plant costs are unlikely to be substantially affected by the heat exchanger solutions. For the purposes of a natural circulation feasibility evaluation and an initial heat exchanger optimization, a detailed

plant investment evaluation was considered unnecessary and beyond the scope. To find conservative upper-limit cost figures, the base C_{SMR} cost was not adjusted for the RPV, CV, heat exchanger, and partial excavation costs. These costs, as obtained in this study, were simply added to the total scaled C_{SMR} figure.

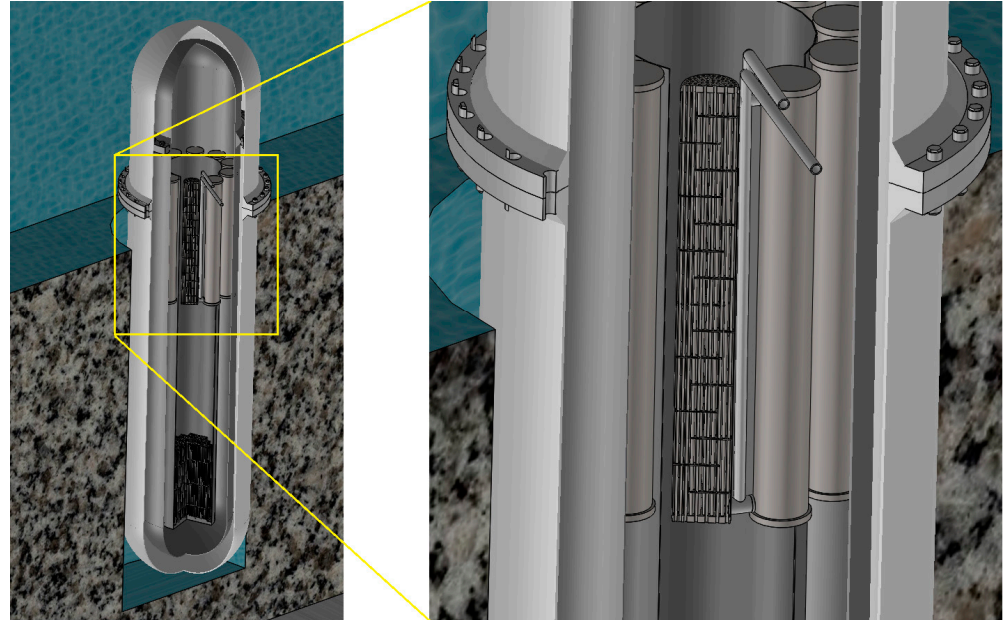


Figure 3. Reactor pool, containment vessel, and pressure vessel concept.

The cost estimates of the heat exchanger and pressure vessels are based on mechanical sizing, performed similarly to [29]. Precise design to any one current pressure vessel code was considered unnecessary for the purposes of this study; instead, the 1996 Finnish pressure vessel code [30] is used to estimate the dimensions and masses of the main parts of the heat exchangers and the RPV and CV. ASTM 316L stainless steel (X2CrNiMo-17-13-3) was used as material for all said components. The fixed parameter values used in mechanical and thermal calculations are summarized in Table 3 below.

Table 3. Main modeling assumptions for mechanical design and thermohydraulic model.

Property	Unit	Value
Corrosion allowance ¹	mm	0.0
Manufacturing tolerance ¹	mm	2.0
Material design stress, ASTM 316L	MPa	141
Young's modulus	N/mm ²	186.9 [31] ²
Poisson's ratio	-	0.268 [31] ³
Density	kg/m ³	7890
Baffle plate thickness	mm	10.0
Minimum tube-to-shell clearance	mm	15.0

¹ not applied on heat transfer tubes. ² linear interpolation between 150 °C and 260 °C values. ³ linear interpolation between 150 °C and 200 °C values.

The sizing is based on 150 °C/5 bar maximum operating conditions in the RPV and a safety factor of 2 for the pressure, and 4 bar(g) maximum pressure in the secondary circuit. Design values of $-1.0/+0.4$ MPa(g) for shell pressure and 180 °C were thus considered for the heat exchangers. For the RPV, the design pressures were $-0.4/+1.0$ MPa(g), and for the CV $-0.25/+0.4$ MPa(g). The 0.4 MPa for the RPV outside and CV internal pressure is set by the possibility of leakage in secondary water pipes pressurizing the containment vessel, and the 0.25 MPa for the maximum hydrostatic pressure at the CV bottom depth. The sizing procedure is described in more detail in Appendix A.

2.3.1. Heat Exchanger Cost Model

The heat exchanger manufacturing cost $C_{\text{man,HX}}$ is estimated via a simplified version of the model of Caputo et al. [32]. The material and processing costs are evaluated separately, and the equipment FOB cost C_{FOB} is obtained by adding the overhead costs, contingency, and manufacturer's profit, estimated at 30%, 5%, and 10% of the FOB, respectively, and a value-added tax of 24%. The total capital investment of the 16 heat exchangers is then determined using a factor of 3.3, according to Sinnott [27]:

$$C_{\text{man,HX}} = C_{\text{mat,HX}} + C_{\text{pr,HX}}, \quad (3)$$

$$C_{\text{FOB,HX}} = \frac{C_{\text{man,HX}}}{1 - 0.30 - 0.05 - 0.10} \cdot 1.24, \quad (4)$$

$$C_{\text{TCl,HX}} = 16 \cdot 3.3 C_{\text{FOB,HX}}. \quad (5)$$

The material costs are dominant in the manufacturing cost. From the mechanical sizing results, the component volumes are obtained and, thereby, the masses. The basic price of 316 L steel is assumed at 6.09 €/kg for all parts except the tubes; seamless drawn tubing is considerably more expensive at 29 €/kg. Material is obtained in the shape of rectangular plates, pipes, tubes, and rods. During processing, some material becomes scrap; a scrap metal price of $c_{\text{sh}} = 1.6$ €/kg is assumed. The material cost calculation process of different components is described in more detail in Appendix B.

Once the dimensions are known, the processing cost can be estimated. The processing cost evaluation is a simplified version of that described in [32]. In segmentally baffled STHs, the processing costs related to baffles represent over half of the total processing cost. The baffle-related costs (cutting, beveling, drilling, and tube bundle assembly) were, thus, modelled similarly to [32] by estimating the total processing length L_{pr} and speed v_{pr} to obtain the processing time $t_{\text{pr}} = L_{\text{pr}}/v_{\text{pr}}$, specific cost per time c_{pr} , and, from there, the total cost $C_{\text{pr}} = c_{\text{pr}} t_{\text{pr}}$. The sum of other processing costs was estimated at 10% of the material cost $C_{\text{mat,HX}}$ based on the results of [32]. The total sum of processing costs of the different operations x are then calculated as

$$C_{\text{pr,HX}} = \sum_x \left[c_{t,x} \left(\frac{L_x}{v_x} + t_{\text{su},x} \right) \left(\frac{1\text{h}}{60\text{ min}} \right) \right] + 0.10 C_{\text{mat,HX}}, \quad (6)$$

where $t_{\text{su},x}$ is the set-up time for each operation x , and the final term is the approximate cost of all other manufacturing processes, estimated at 10% of material cost. The equations and assumptions used for processing cost estimation are summarized in Appendix C.

2.3.2. Reactor Pressure Vessel and Containment Vessel Cost Models

The RPV and CV both consist of a cylindrical section, hemispherical top, and bottom heads. A detailed design of the RPV is not yet available at this stage. The costs due to the various features added to the bare pressure vessel components were estimated as representing a similar fraction of the total material cost as in the NuScale SMR concept, which utilizes a somewhat similar elongated RPV [33].

The dimensions of the RPV and the CV are found by estimating the straight section of the RPV cylinder to continue 1.5 m above the top of the heat exchanger and a distance $\Delta H - 0.5D_{\text{RPV}}$ below (see Figure 4). A 0.5 m gap separates the CV inner surface from the RPV outer surface at the sides and bottom, i.e., $D_{\text{CV,i}} = D_{\text{RPV,o}} + 1.0$ m. The cylindrical part of the CV shell is 1 m longer than the RPV.

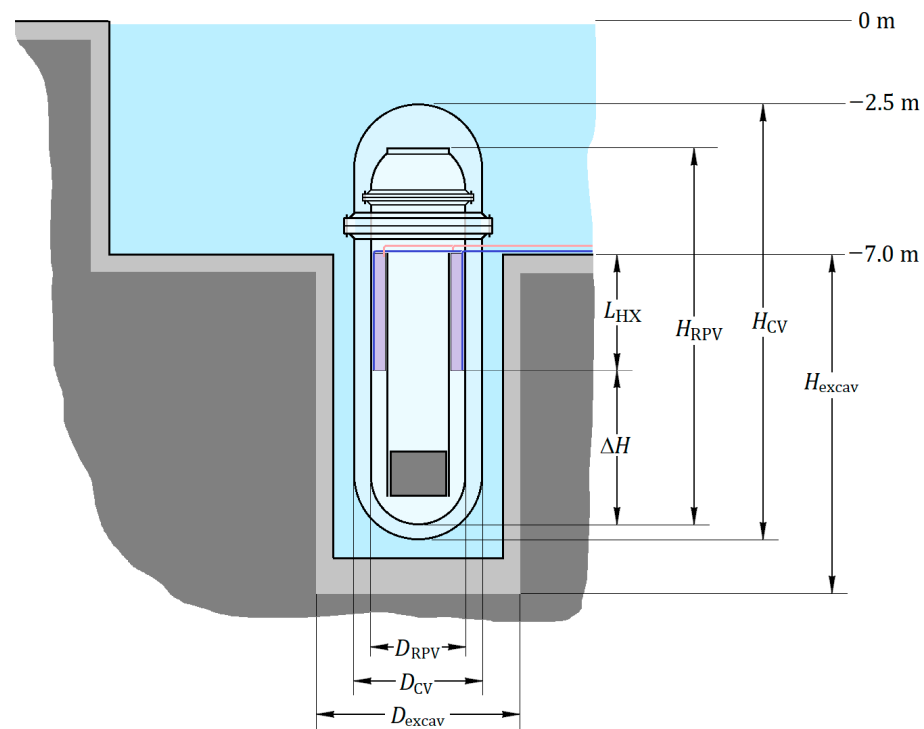


Figure 4. Main dimensions of reactor pool, containment vessel (CV), reactor pressure vessel (RPV), primary heat exchangers (HX), and the excavated cylindrical cavity below main pool bottom.

Using the price data in [34], a value of 13.6 €/kg is obtained for the cylindrical shell and the heads when corrected for the 2021 producer price index for the manufacture of fabricated metal products, excluding machinery [35]. This increases to 18.3 €/kg with an estimated 4.7 €/kg cost difference between carbon steel and ASTM 316L. The other vessel components, e.g., possible conical sections, flanges, and openings (but not the core and related equipment), were estimated to constitute 40% of the NuScale RPV cost [33,34]. With this assumption that the shell and heads, whose mass is obtained from the sizing, constitute 60% of the total material costs as in [34], the adjusted material cost that can be used to obtain the pressure vessel cost with the mass of the main parts (cylindrical shell and heads); m_{s+h} , is obtained from

$$c_{\text{mat}} = \frac{c_{\text{mat, s+h}} m_{\text{s+h}}}{0.60} \quad (7)$$

as 30.54 €/kg. The manufacturing costs of the RPV and CV are then found, assuming a work-to-material cost ratio of 0.657 [34]. Although the stainless-steel vessel does not need cladding, for a conservative estimate, the work cost was not adjusted down. FOB and TCI costs are estimated using similar mark-up and installation factors as with the heat exchangers, Equations (4) and (5).

2.3.3. Reactor Pool Cost Model

The 7-m-deep main pool is unaffected by the heat exchanger design and is considered part of the fixed-cost C_{SMR} . Only the cost of the cylindrical cavity extending below the main pool, C_{cav} , varies as a function of the heat exchanger dimensions and the height DH to the RPV bottom and is, thus, evaluated in the cost model. This consists of two components: excavation C_{excav} , and wall construction $C_{\text{cav,w}}$.

The cavity has a 0.5-m-thick steel-reinforced concrete wall with 10 mm steel lining. The concrete cost is the sum of material and labor costs per m^3 . The material cost is obtained from the rebar-to-concrete mass ratio r , 0.11 for reactor buildings in Gen IV nuclear systems, the specific costs from [36], index-corrected according to [37]. Excavation cost is obtained from the estimated cavity volume, as described in Supplementary Material S1.

2.3.4. Decision Variables and Constraints

The decision variables and their feasible ranges are listed in Table 4. In addition to the feasibility ranges, the following additional constraints are considered:

- Maximum shell-side velocity $w_{sh,max} < 1.5$ m/s;
- Maximum shell-side pressure drop $Dp_{sh} < 1.0$ bar;
- Primary water inlet temperature $T_{h,in} < 150$ °C;
- Tube pitch ratio $1.25 \leq P/d_o \leq 1.45$;
- RPV straight length below heat exchanger $\Delta H < 2.0$ m.

Table 4. Decision variables in the optimization, and their feasible regions.

Variable	Unit	Range
Tube layout θ_{tp}	°	{30, 60}
Baffle cut BC	-	$0.15 \leq BC \leq 0.40$
Shell outer diameter and wall thickness $D_{sh,o} \times s_{sh}$	mm	{273.0 × 7.8, 323.9 × 8.4, 355.6 × 9.5, 406.4 × 9.5} ¹
Tube diameter d_o	mm	{8, 10, 12, 14, 15, 16, 18}
Tube spacing $P-d_o$	-	$3.2 \leq P/d_o \leq 5.0$
Tube length L_{tb}	m	$2 \leq L_{tb} \leq 6$
Sealing strip pairs N_{SS}	-	$0 \leq N_{SS} \leq 7$
Baffle/shell ratio S_{bf}/D_{sh}	mm	$0.20 \leq S_{bf}/D_{sh} \leq 1$
RPV height H_{RPV}	m	$4.00 \leq H_{RPV} \leq 12.00$

¹ DN 250, 300, 350 or 400, Sch 30.

2.4. Thermohydraulic Model

The heat exchanger model solves the heat exchanger performance as a rating problem for a given geometry. Because the operation is based on the natural circulation of the hot fluid, only the inlet state and mass flow rate of the cold flow and the total heat transfer rate are fixed and known. The heat exchanger performance (heat transfer and pressure drop) and the inlet and outlet state both affect each other, requiring an iterative solution to determine the operating point. In addition to the heat exchanger itself, the reactor core pressure drop also affects circulation. Pressure drops in the riser and downcomer outside of the core and the heat exchangers are considered negligible.

The solution process, shown as a flow chart in Algorithm 1, is based on two nested iteration loops. The outer loop adjusts the primary water inlet temperature to match the $\Phi_{tgt} = 3.125$ MW (50MW/16) target heat rate in a heat exchanger, while the inner adjusts the primary water flow to match the total pressure drop (reactor core plus heat exchanger), with the Δp_{tgt} available from the natural circulation. Damping factors α are used and adjusted during the iteration to ensure convergence. The primary water outlet temperature in step 3.1.3 is solved from tube outside area A_o and overall heat transfer coefficient U using the ε - NTU method, based on dimensionless parameters NTU , ε , and C^* :

$$NTU = \frac{UA_o}{(\dot{m}c_p)_{\min}} = \frac{UA_o}{\dot{C}_{\min}} \quad (8)$$

$$C^* = \frac{\dot{C}_{\min}}{\dot{C}_{\max}} \quad (9)$$

$$\varepsilon = \frac{\Phi}{\Phi_{\max}} = \frac{\dot{C}_c(T_{c,out} - T_{c,in})}{\dot{C}_{\min}(T_{h,in} - T_{c,in})} \quad (10)$$

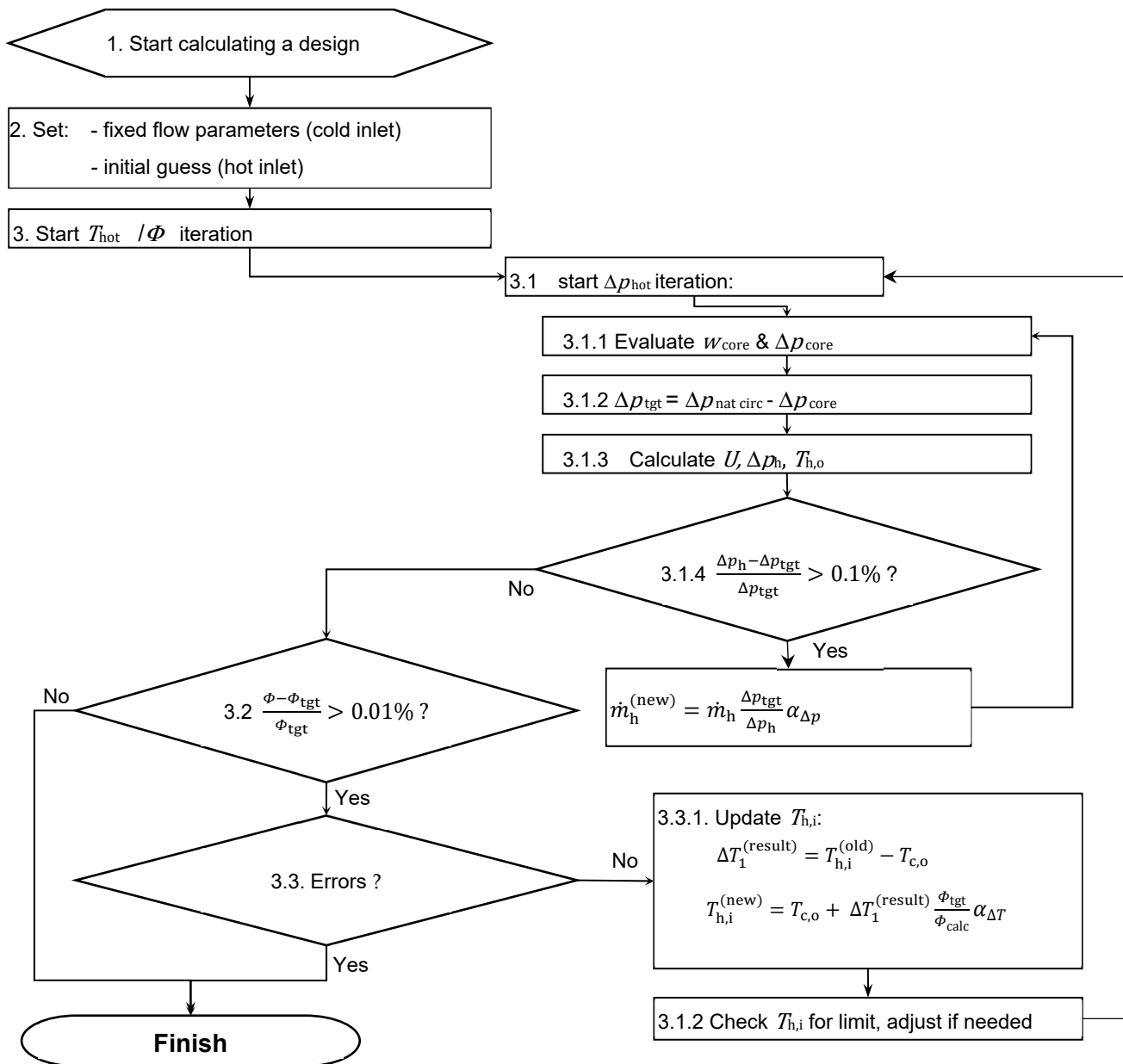
$$\varepsilon_{\text{countr}} = \frac{1 - e^{-NTU(1-C^*)}}{1 - C^*e^{-NTU(1-C^*)}} \quad (11)$$

The overall heat transfer coefficient U is found from

$$U = \left[\frac{d_o}{d_i} \left(R''_{tf,i} + \frac{1}{h_i} \right) + \frac{d_o \ln \frac{d_o}{d_i}}{2k_w} + R''_{tf,o} + \frac{1}{h_o} \right]^{-1}, \quad (12)$$

where $R''_{tf,i}$ and $R''_{tf,o}$ are inside and outside fouling resistances and R''_w , the tube wall resistance. The fouling is estimated to be similar to a steam power plant low-pressure feed heater. Based on the Heat Exchanger Institute’s recommendation [38] and a nuclear power plant feed heater diagnostics system [39], values of $R''_{tf,i} = 3.5 \cdot 10^{-5} \text{ m}^2\text{K/W}$ (feed heater fouling resistance 1 year from start-up) and $R''_{tf,o} = 5.3 \cdot 10^{-5} \text{ m}^2\text{K/W}$ (feed heater drain cooling section tube outside resistance) are used.

Algorithm 1. Iteration process for the heat transfer model to evaluate a single load point defined by the DH production and the supply and return temperatures.



2.4.1. Tube-Side Heat Transfer Coefficient

Ideally, the tube-side flow should be fully turbulent, with Reynolds number $Re > 10^4$. This ensures good, predictable heat transfer and a small area. Unfortunately, with natural circulation, this cannot be guaranteed: transition or fully laminar flow is a risk, especially at part-load when using small tubes. Small-diameter tubes can also result in a hydraulically smooth surface condition not being met. This can be advantageous, as the partially rough flow regime increases the heat transfer coefficient, although, unfortunately, the literature on the partially rough regime heat transfer is both dated and sparse. As none of the aforementioned conditions can be ruled out, all are implemented in the model.

The tube inside heat transfer coefficient h_i in transition and fully turbulent regime ($Re > 2300$) is evaluated primarily using a variant of the Gnielinski correlation [40],

$$Nu_{\text{Gniel}} = \frac{h_i d_i}{k_{f,i}} = \frac{0.125 f_D (Re - 1000) Pr}{1 + 12.7 \sqrt{0.125 f_D} (Pr^{2/3} - 1)}, \quad (13)$$

where the Darcy friction factor f_D for hydraulically smooth tubes is obtained from the Bhatti–Shah correlation [41],

$$f_D = 0.00512 + 0.4572 Re^{-0.311}. \quad (14)$$

Equation (13) is said to be valid for $2300 \leq Re \leq 5 \cdot 10^6$; while it can be considered accurate for water at 50–150 °C range at the fully turbulent $Re > 10^4$ regime, yielding almost identical results to the Petukhov–Popov correlation [42] from which it is derived, it is not recommended for the $2300 < Re < 10^4$ transition regime [43] where the flow intermittently switches between laminar and turbulent [44]. Based on this observation in [44], a linear interpolation between fully turbulent $Re = 10^4$ and fully laminar $Re = 2300$ heat transfer coefficient,

$$Nu_{\text{trans}} = (1 - \gamma) Nu_{\text{lam}, Re=2300} + \gamma Nu_{\text{turb}, Re=10^4}, \quad (15)$$

where the intermittency factor γ is

$$\gamma = \frac{Re - 2300}{10^4 - 2300}, \quad (16)$$

has been proposed in [45] as cited in [46]. To find a conservative estimate for the purpose of natural circulation feasibility evaluation, heat transfer in the $2300 < Re < 10^4$ regime is modelled by evaluating the Nu with both (13) and (15), and using the lower result.

The turbulent $Nu_{\text{turb}, Re=10^4}$ in Equation (15) is obtained with Equation (13). The $Nu_{\text{lam}, Re=2300}$ depends on the tube wall boundary condition. Considering constant heat flux a better approximation than the constant temperature in a counter-current heat exchanger, the laminar Nu is thus evaluated according to [46]:

$$\begin{aligned} Nu_{\text{lam}} &= \left\{ \overline{Nu}_{\text{lam},1}^3 + 0.6^3 + [\overline{Nu}_{\text{lam},2} - 0.6]^3 + \overline{Nu}_{\text{lam},3}^3 \right\}^{1/3}; \\ \overline{Nu}_{\text{lam},1} &= 4.364; \\ \overline{Nu}_{\text{lam},2} &= 1.953 \left(Re Pr \frac{d_i}{L_{\text{tb}}} \right)^{1/3}; \\ \overline{Nu}_{\text{lam},3} &= 0.924 Pr^{1/3} \left(Re \frac{d_i}{L_{\text{tb}}} \right)^{1/3}. \end{aligned} \quad (17)$$

When surface roughness protrusions extend beyond the laminar sublayer in turbulent flow, the hydraulically-smooth surface approximation no longer applies. Roughness effects are correlated with a roughness Reynolds number e^+ ,

$$e^+ = \frac{e}{d_i} Re \sqrt{\frac{C_f}{2}}, \quad (18)$$

where e is the sand-grain roughness and C_f the Fanning coefficient of friction. Although fully rough ($e^+ > 70$) flow is unlikely, partially rough ($5 < e^+ < 60-70$) [43] cannot be ruled out. In this region, the turbulent Nu is adjusted according to Norris [47] as cited in [48],

$$Nu_{\text{rough}} = Nu_{\text{smooth}} \left(\frac{C_{f,\text{rough}}}{C_{f,\text{smooth}}} \right)^{0.68 Pr^{0.215}}, \tag{19}$$

where the C_f is obtained from the explicit approximation of the well-known iterative Colebrook-White equation according to Chen [49],

$$\frac{1}{\sqrt{C_f}} = 3.48 - 1.7372 \ln \left\{ \frac{2e}{d_i} - \frac{16.2426}{Re} \ln \left[\frac{\left(\frac{2e}{d_i} \right)^{1.1098}}{6.0983} + \left(\frac{7.149}{Re} \right)^{0.8981} \right] \right\}. \tag{20}$$

2.4.2. Shell-Side Heat Transfer Coefficient

Calculating the shell-side heat transfer coefficient h_o follows the Bell-Delaware method, using the Nu correlations and correction factors f according to [50] in

$$Nu_o = \frac{h_o d_o}{k_{f,o}} = f_A f_N f_G f_L f_B f_P \left(0.3 + \sqrt{Nu_{\text{lam}}^2 + Nu_{\text{turb}}^2} \right), \tag{21}$$

where the factors f are for tube arrangement (f_A), turbulence development (in multi-baffled heat exchangers $f_N = 1$), deviation of the shell-side main flow, path A in Figure 5, from pure cross flow (f_G), bypass flow B (f_B), leakage flows C and D through baffle-shell and baffle-tube gaps (f_L), and fluid property variation (f_P). Except for fluid property variation f_P , and f_B at extremely low- Re flows, these are determined from the geometry alone, unaffected by flow parameters. The equations for obtaining these are listed in [50].

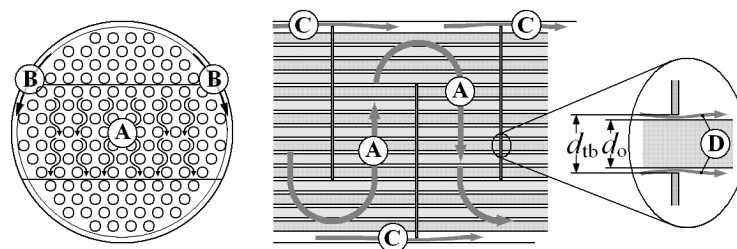


Figure 5. Main flow paths in shell-side flow.

The turbulent and laminar Nu in Equation (14) are obtained from Equations (22) and (23),

$$Nu_{\text{lam}} = 0.664 \sqrt{Re_{\psi,1}} \sqrt[3]{Pr} \tag{22}$$

$$Nu_{\text{turb}} = \frac{0.037 Re_{\psi,1}^{0.8} Pr}{1 + 2.443 Re_{\psi,1}^{-1} (Pr^{2/3} - 1)} \tag{23}$$

with $Re_{\psi,1}$ defined as

$$Re_{\psi,1} = \frac{w l \rho}{\psi \mu}, \tag{24}$$

where w is the cross-flow velocity at shell centerline between two baffles without tubes, l the streamed length $\frac{1}{2} \pi d_o$, ρ the density, μ the dynamic viscosity, and ψ a void fraction to account for the fraction of free flow area left between the tubes as defined in [50].

For shell-side calculation, the number of tubes N_{tb} is estimated according to [33] as

$$N_{\text{tb}} = 0.319 \cdot \left(\frac{1.25}{P/d_o} \right)^2 \cdot \left(\frac{D_{\text{OTL}}}{d_o} \right)^{2.142}, \tag{25}$$

where D_{OTL} is the outer tube limit (see Figure 6) and P the tube pitch; of these the number of tubes in the tube window $N_{tb,w}$ is estimated as the same as the ratio of the bundle segment area in the window A_W , based on segment height h_{bndl} and diameter D_{OTL} , to the area of the whole circular bundle of same diameter D_{OTL} .

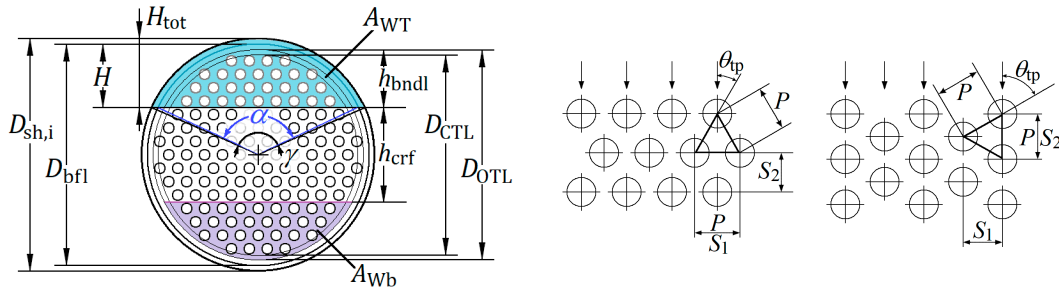


Figure 6. Shell-side baffle and bundle geometry variables.

2.4.3. Pressure Drop, Heat Exchanger

The tube-side Δp_i is found using the Darcy-Weisbach equation,

$$\Delta p_i = \frac{\rho_i w_i^2}{2} \left(\frac{f_D L}{d_i} + \sum K \right), \tag{26}$$

where L is the tube length, the loss coefficients K are $K_{i,in}$ and $K_{i,out}$ into and out from the tubes, respectively. Constant $K_{i,out} = 1$ is assumed, while $K_{i,in}$ is determined as a function of P and θ_{tp} [51]. When the tube is hydraulically smooth, $e^+ < 5$, f_D is obtained from Equation (14), otherwise as $f_D = 4C_f$, with the C_f from Equation (20).

Shell-side pressure drop Δp_o is the sum of Δp in cross-flow between baffles Δp_Q , entry and exit cross flow sections Δp_{QE} , baffle windows Δp_W , and at the nozzles Δp_{nzl} :

$$\Delta p_o = (N_{bf} - 1)\Delta p_Q + 2\Delta p_{QE} + N_{bf}\Delta p_W + \Delta p_{nzl}, \tag{27}$$

where N_{bf} is the number of baffles; the different components are depicted in Figure 7. The calculation process follows the methodology described in [52].

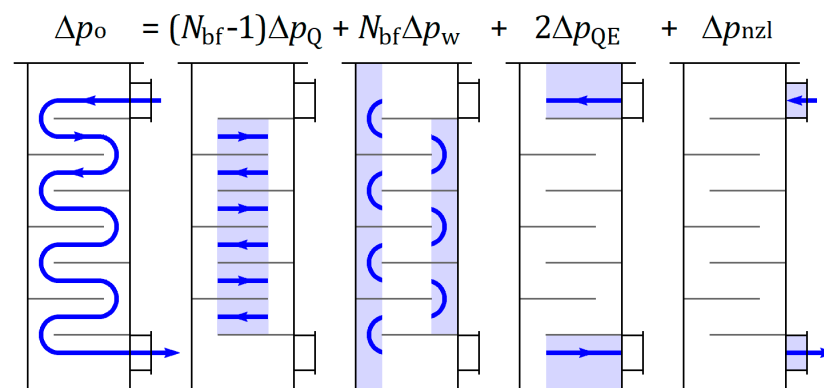


Figure 7. Shell-side pressure drop components, Equation (27).

2.4.4. Pressure Drop, Reactor Core

The reactor core consists of 37 otherwise typical 17×17 pressurized water reactor (PWR) fuel assemblies, but with a shorter 1-m active length (total length assumed $L_{core} = 1.3$ m), corresponding to the LDR-50 DH reactor concept [14,15]. The core pressure drop Dp_{core} consists of the sum of fuel rod surface friction losses, and form losses due to the spacer grids, top and bottom nozzles, and the inlet contraction and outlet expansion losses, and the gravity loss. The gravity loss is accounted for by considering the riser height down to midpoint of the core in determining the natural circulation driving force.

The friction and form losses are evaluated with Equation (26) using the mean \bar{w}_{core} as velocity, and L_{core} and subchannel hydraulic diameter d_h as the length and diameter [53]. Friction factor f_D is obtained using Equation (16) for fully turbulent flow, $64/Re$ for laminar. At $2300 < Re < 10^4$, linear interpolation between $64/2300$ and Equation (16) at $Re = 10^4$ is used.

All form losses including the grid spacers, core top and bottom structures, and inlet (contraction) and outlet (expansion), are estimated with loss coefficients. Core inlet and outlet loss coefficients are estimated at 0.5 and 1.0, respectively [53]. For the grid spacers and top and bottom structures the loss coefficients are obtained using the correlation for PWR spacers [53],

$$K = (2.75 - 0.27 \log_{10} Re) \frac{\varepsilon}{(1 - \varepsilon)^2}, \quad (28)$$

where ε is the ratio between the projected area of the obstruction (grid) to the flow area without the obstruction.

The loss coefficients are determined assuming the fuel assemblies are shortened versions of the AP1000 fuel assemblies. While the details of the grid spacers and other obstructions are not known, the number and type of spacers as well as the typical pressure drop in AP1000 conditions are known [54]. From this, representative values for ε can be found, which are then used in Equation (28) for the shorter fuel design in the DH reactor conditions, considering a total of three grid spacers, and top and bottom structures.

2.5. Modified Cuckoo Search Algorithm

The Cuckoo Search (CS) is a metaheuristic global optimizer [55] metaphorically based on the well-known brood parasitism of cuckoo birds [56], as well as a search pattern known as Lévy flights observed in many foraging species in nature [56]. The CS is a population-based method; each candidate solution to an optimization problem represents a cuckoo egg. Each egg is represented by a vector \mathbf{x} of D decision variable values.

The literature on the CS is unfortunately somewhat contradictory. Earlier two very similar, one somewhat modified, and a fourth, significantly different variant, all described by the authors of the method as simply “Cuckoo Search”, were identified. The differences were described in [22] and in further detail in [17]. The first three variants, labelled CS1 sub-variants [17], proved unsuccessful in heat exchanger optimization, but the fourth, CS2, was highly successful, and was modified further into the CS3 in [17]. Both CS2 and CS3 borrow heavily from another well-known metaheuristic, the differential evolution (DE). In this study, the CS3 was implemented.

Like all CS variants the authors are aware of, the CS3 consists of two steps. The first is based on DE [57]. The differences to DE are the use of a randomized mutation weight, and each target vector \mathbf{x}_i against which the trial vector \mathbf{u}_i competes serving also as the base vector in generating \mathbf{u}_i , rather than the latter being separately and randomly selected. All population members serve as target vector once per iteration.

In [17] the greedy local-to-best mutation strategy proved fastest, while still remaining robust. In this case, the greater number of decision variables, many of which are discrete, is likely to produce a severely discontinuous and multi-modal objective function topology. As a thorough meta-optimization was ruled beyond the scope, the more conservative CS3/rand/1/bin was selected over the greedy local-to-best variant. The rand/1/bin trial vector \mathbf{u}_i generation gives each decision variable d a value according to

$$u_{i,d}^G = \begin{cases} x_{i,d}^G & \text{if } \varepsilon_d \leq CR \\ x_{i,d}^G + F_d (x_{r1,d}^G - x_{r2,d}^G) & \text{otherwise} \end{cases} \quad (29)$$

where the mutation weight F_d is drawn from a size D -dimensioned normal-distributed random-number vector \mathbf{F} (mean = 0.8), and ε_d is a uniform-distributed random num-

ber, $\varepsilon_d \in (0,1)$. For a rotationally invariant search effective at non-separable problems, the crossover probability CR should have a small value.

The second step is a Lévy-distributed random walk. While these Lévy flights appear generally less efficient than the differential mutation at most problems, they have one important advantage: retaining a capability for long leaps in the objective function landscape even after the population has converged into a small area. This preserves some global search capability. In the CS3 variant of Cuckoo Search, the tuning parameter p_a (“switching probability”) determines the fraction of population on which the Lévy flights are implemented. After the differential mutation step, the population is ranked, and a fraction p_a of the worst eggs are subjected to Lévy flights. Each egg serves once as a base vector \mathbf{x}_i , using its distance to a randomly chosen vector \mathbf{x}_{r1} to generate a trial vector \mathbf{u} ,

$$\mathbf{u} = \mathbf{x}_i + \alpha \cdot (\mathbf{x}_i - \mathbf{x}_{r1}) \circ \mathbf{s} \circ \mathbf{n}, \quad (30)$$

where α is a scaling factor, \mathbf{s} a Lévy-distributed step size vector, \mathbf{n} a vector of normal-distributed random numbers, and operator \circ the Hadamard product. Considering the role of the Lévy flights as one of global search to prevent stagnation on local optima, even when the distance $\Delta \mathbf{x}_{\text{best}}$ is small, a comparatively large value of $\alpha = 0.1$ is used. The vector \mathbf{s} is determined using the Mantegna’s algorithm [58]

$$\mathbf{s} = \mathbf{p} \circ \mathbf{q}^{-1/\beta}, \quad (31)$$

where \mathbf{p} and \mathbf{q} are normal-distributed random-variable vectors of size D , a mean of zero, and variances of 1 and σ^2 , respectively, with

$$\sigma^2 = \left[\frac{\Gamma(1 + \beta)}{\beta \cdot \Gamma\left(\frac{1}{2} + \frac{1}{2}\beta\right)} \cdot \frac{\sin\left(\frac{1}{2}\pi\beta\right)}{2^{\frac{1}{2}(1+\beta)}} \right]^{-1/\beta}. \quad (32)$$

Based on recommendation in [56], Lévy exponent of $\beta = 1.5$ is used. A trial vector is evaluated by competition against the original base vector; the one with better objective function value survives to the next generation. The pseudo-code of CS3/rand/1/bin is found in Appendix D (Algorithm A1), and MATLAB code of the algorithm in Supplementary Material S3. A population size of $NP = 45$, crossover probability $CR = 0.1$, and $p_a = 0.20$ were used in all runs.

Due to the multi-constrained nature of the problem, often all members of the initial population are infeasible. Constraints are handled by penalty functions, implemented so that an infeasible solution always loses to any feasible one, no matter how poor; between two infeasible solutions, the one in breach of higher number of constraints always loses; and between two in breach of one constraint, the one in greater magnitude of violation is likely to lose. This ensures a rapid convergence towards feasible regions.

3. Results

The convergence behavior of the CS3 algorithm appeared robust, albeit somewhat slow, and requiring a fairly large population size of $5D$. While twice greater than the $2.5D$ population and a greedier mutation strategy with the lower-dimensioned, less multimodal condenser optimization in the original introduction of the CS3, this is still half of what is common with the classic DE on which the CS3 is based. The convergence behavior at the three cases with 10 trial runs per case can be seen in Figure 8.

Once the number of objective function evaluations (NFE) reached 50,000, the search was terminated and re-started with halved population size and a region limited around the solutions found by the 10 runs for another 10,000 evaluations to obtain the exact solutions, listed in Table 5. The full data are available from Supplementary Material S2.

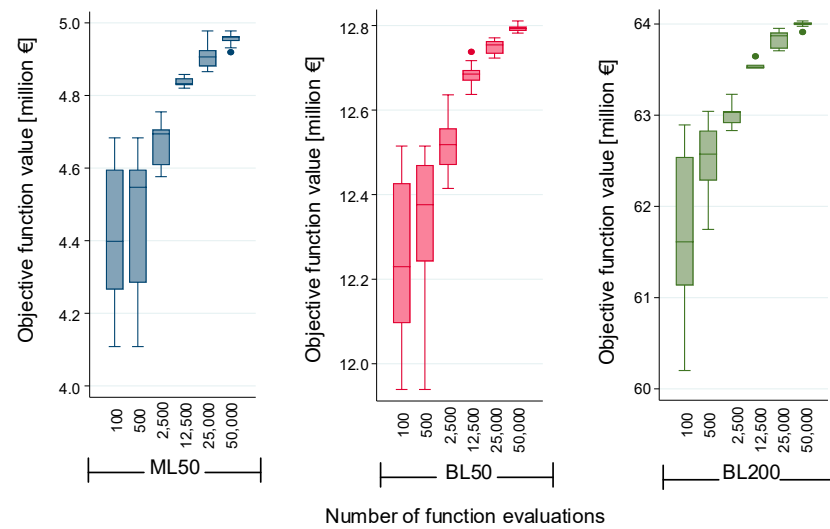


Figure 8. Optimization convergence behavior with 10 optimization runs of the 3 cases.

Table 5. Optimization results.

Variable		Unit	Case BL200		Case BL50		Case ML50	
Number of reactors		-	4		1		1	
Annual net cash flow C_{net}		10^6 €	63.9		12.4		5.0	
Cost-price of heat ($i = 10\%$)		€/MWh	31.0		39.8		53.2	
Cost-price of heat ($i = 5\%$)		€/MWh	22.8		28.5		37.6	
Decision variables	Tube layout θ_{tp}	°	60		60		60	
	Baffle cut BC	-	0.152		0.152		0.184	
	Shell outer diameter and wall thickness $D_{sh,o} \times s_{sh}$	mm	406.4×9.5		406.4×9.5		406.4×9.5	
	Tube diameter d_o	mm	12		12		12	
	Tube pitch ratio P/d_o	-	1.267		1.267		1.267	
	Tube length L_{tb}	m	2.969		2.969		2.969	
	Sealing strip pairs N_{SS}	-	3		3		2	
	Baffle/shell ratio S_{bf}/D_{sh}	mm	0.48		0.44		0.47	
Riser height H_{riser}	m	5.566		5.552		5.600		
Sizes and costs	Total heat transfer area A	m^2	16×50.4		16×50.3		16×50.4	
	RPV height \times diameter \times thickness	m	$9.82 \times 2.76 \times 0.023$		$9.81 \times 2.77 \times 0.023$		$9.87 \times 2.77 \times 0.023$	
	CV height \times diameter \times thickness	m	$12.2 \times 3.82 \times 0.031$		$12.3 \times 3.84 \times 0.031$		$12.3 \times 3.83 \times 0.031$	
	FOB cost, heat exchangers	10^6 €	0.739 ¹		0.745		0.728	
	FOB cost, RPV	10^6 €	1.957 ¹		1.969		1.979	
	FOB cost, CV	10^6 €	4.468 ¹		4.491		4.508	
	Reactor pool cavity cost	10^6 €	3.068 ²		0.981		0.989	
Pumping cost	10^6 €	0.464 ²		0.117		0.088		
Flow parameters			Winter LP1	Summer LP6	Winter LP1	Summer LP6	Winter LP1	Summer LP6
	Primary water inlet/outlet $T_{h,in/out}$	°C	150/102	143/94	150/105	143/97	150/102	107/84
	Primary water in-tube velocity w_{tb}	m/s	0.44	0.43	0.44	0.43	0.44	0.25
	Primary water Re at tube outlet	-	15,068	13,659	15,017	13,611	15,199	7236
	Primary water Dp , tubes	mbar	8.6	8.4	8.6	8.4	8.6	3.5
	Primary water Dp , core	mbar	5.2	5.1	5.2	5.1	5.1	2.1
	Secondary (shell-side) Dp	mbar	252	253	281	283	228	36
	Tube-side heat transfer coefficient h_i	W/m ² K	4389	4257	4380	4248	4411	2082
	Shell-side heat transfer coefficient h_o	W/m ² K	10,293	9968	10,552	10,217	9971	4800
Overall heat transfer coefficient U	W/m ² K	1789	1750	1794	1756	1783	1026	

¹ per single reactor; ² for all 4 reactors.

The results show that the primary-circuit natural circulation design appears feasible for a DH reactor design, including partial-load operation. The designs are very similar. All designs use small 12 mm tubes—the smallest diameter, where the 3.2-mm tube sheet ligament minimum does not yet significantly increase the tube pitch ratio from its 1.25 minimum. The small tube and large shell diameters allow for placing the necessary heat transfer surface in a smaller length. There is a 2.6-m empty height in the RPV up to the bottom of the heat exchangers: the fully cooled, dense primary fluid there adds to the natural circulation force more than a similar RPV height with taller heat exchangers would.

Clear differences only appear in the flow parameters of the summer load point LP6, where the operating conditions of BL cases remain similar to the winter LP1, whereas in the case of ML, the reduced load results in clearly reduced flow rates and primary-side temperature. This results in reduced heat transfer coefficients and pressure drops (Figure 9), and transition-regime flow at the tube exit. All other cases, and most load points of ML50, are fully turbulent.

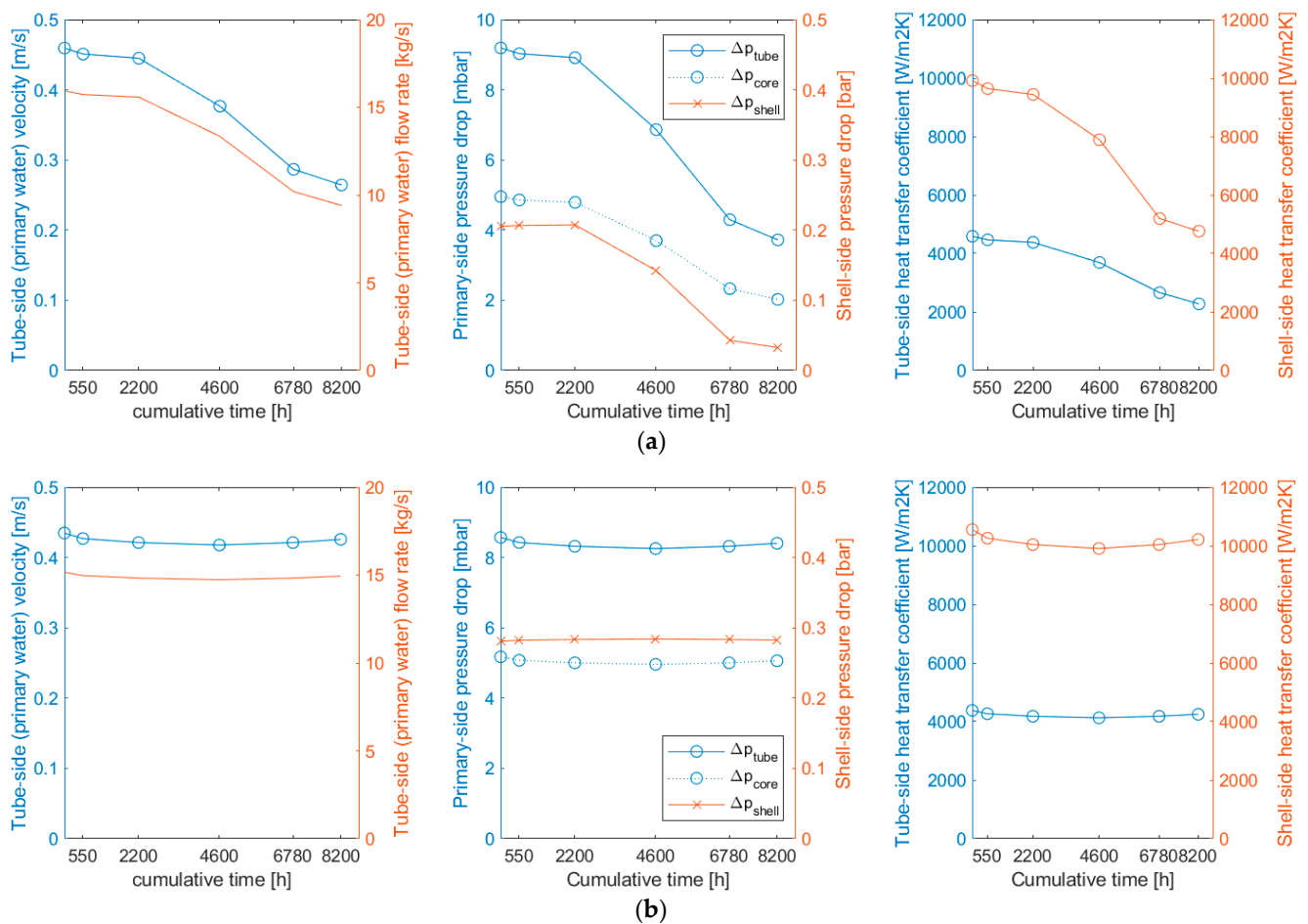


Figure 9. Annual variation of main flow parameters in case ML50 (a) and BL50 (b). All data, except core D_p , refers to conditions in a single heat exchanger (one of 16). Case BL200 exhibits similar behavior to BL50.

Another clear conclusion of the results is that the reactor pressure vessel and containment vessel costs far exceed the costs of the heat exchangers themselves. The cost breakdowns are shown in Figure 10 in terms of both TCIs and produced heat cost-price.

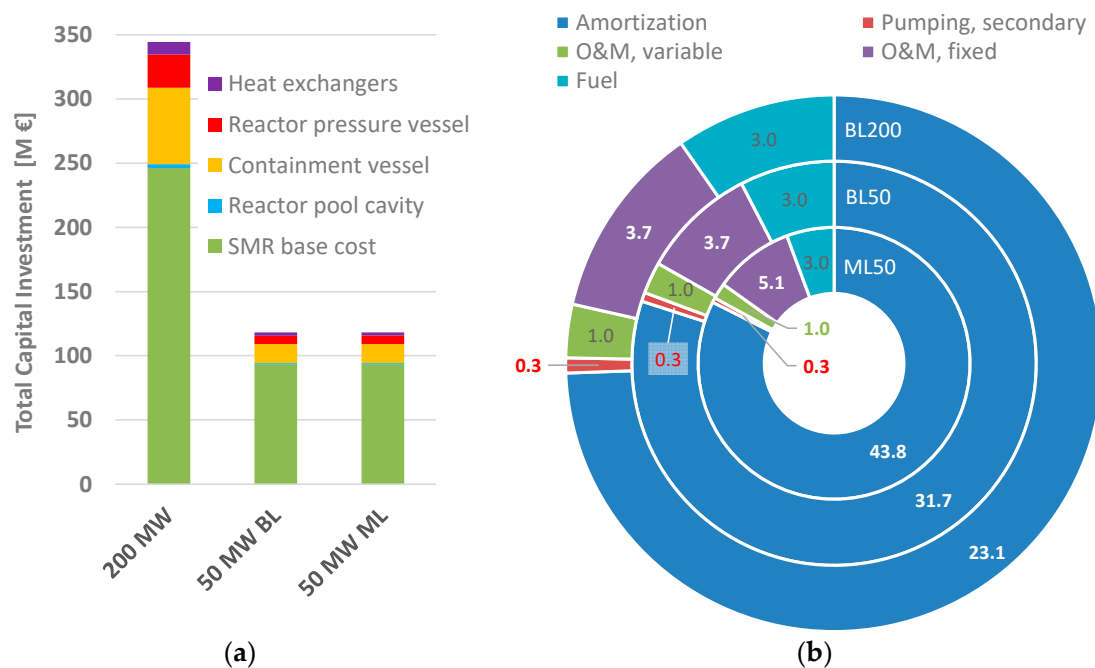


Figure 10. Components of investment cost in M€ (a) and district heat cost-price in €/MWh (b).

As the heat exchanger design clearly will impact the dimensions and cost of vessels (and the pool cavity), but the designs of these components are still at a very preliminary stage, the initial heat exchanger design cannot be considered final. Finally, the optimal design can only be found once the designs and cost models of said components approach the final stage as well, resulting in an iterative design process.

4. Discussion

The results indicate that a small district heating reactor operating in the natural circulation principle is a feasible concept under different load profiles and operating conditions. While minor differences between the configurations optimized for different scales and load profiles were found, the differences are small enough to be arguably negligible, permitting a single standardized design of all main components: the heat exchangers, the reactor pressure vessel (RPV), and the containment vessel (CV).

A central feature of the optimal solution is the compact packaging of the heat transfer surface as high as possible in the RPV downcomer, dividing the total riser height approximately in half between the heat exchangers at the top and empty space filled with fully cooled primary water at the bottom half. This allows to maximize the pressure difference driving the natural circulation.

As the designs of the RPV and CV are not yet finalized, the results obtained here must also be treated as tentative, subject to change, as the designs and cost functions of said pressure vessels, as well as the pool cavity and the reactor core, become more detailed and accurate. The heat exchanger cost model itself, as well as some of the constraints, are currently also still on a general level. In a final design, data on the equipment available to the chosen manufacturers can be used to obtain a design tailored for such. Such final optimization should also consider the reactor pressure and temperature levels, considered as fixed constraints in this initial study, as free decision variables.

In terms of optimizer performance, the modified cuckoo search proved effective. Although considerably more conservative tuning parameters settings were needed than with the condenser optimization for which the method was originally introduced, the population size was still only half of what would typically be required with differential evolution.

Finally, although analyzing the final cost competitiveness of the considered heating reactor concept was not a goal of the work, some conclusions can still be drawn. The obtained annual net cash flow rates were clearly positive for all cases, even though conservative or even pessimistic assumptions were applied throughout the process. The cost-price of the produced heat, 30–55 €/MWh, is well under the average selling price of district heat in Finland. At base-load operation, the 30–40 €/MWh cost-price is broadly similar to what could be obtained using a heat pump system with 880 €/kW_{th} CAPEX and an average of 40 €/MWh purchased electricity price with 20 €/MWh grid and tax costs while avoiding vulnerability to the sometimes very high electricity costs during peak-load conditions.

At mid-load operation, the 35–55 €/MWh heat price is broadly similar to or slightly greater than the cost price for a wood chip-fired heat-only boiler. While biomass-fired heat and power generation are likely to remain important in Scandinavian conditions for the foreseeable future, the availability of sustainably produced solid biofuels for heat generation is limited and likely insufficient to fulfill the heat demands, especially in larger population centers in, e.g., Finland or Sweden. Reactor concepts, such as the one considered in this study, thus, appear economically feasible and potentially important components of a cost-effective, clean energy system.

5. Conclusions

The optimization of the primary heat exchangers of a small, 50-MW district heating reactor circulation natural using a modified cuckoo search algorithm proved successful. The following main conclusions from the study were drawn:

- A natural-circulation concept for a heat-only reactor appears feasible for both steady base-load and load-following operation. The optimized configurations for different scales and load profiles are near-identical;
- Central to the optimized heat exchanger configurations was using small-diameter tubes at minimum allowable tube sheet ligament thickness. The resulting high density of heat transfer area per volume enables keeping the heat exchangers in the upper half of the downcomer, filling the lower half with fully cooled primary water. This maximizes the pressure difference available to drive natural circulation;
- The reactor pressure vessel and containment vessel dominate the cost impact of the heat exchanger designs;
- A heat-only reactor producing hot water at modest temperatures has the potential to be a highly competitive carbon-neutral DH producer. The two central reasons behind this are the lightweight construction possible for a low-temperature, low-pressure concept and the ability to convert the reactor thermal power into an energy product without the heat rejection losses inevitable in an electricity-producing power cycle;
- The modified cuckoo search proved successful for the optimization task, although compared to an earlier condenser optimization study, using considerably more conservative control parameters settings emphasizes robustness over speed.

Supplementary Materials: The following supporting information can be downloaded at: <https://www.mdpi.com/article/10.3390/en16062739/s1>, S1: Reactor pool cavity dimensions and cost model. S2: Optimization results, full data. github.com/jmsaari75/CS3, S3: CS3 optimizer MATLAB code and instructions. github.com/jmsaari75/STHESize, S4: mechanical sizing MATLAB code and instructions.

Author Contributions: Conceptualization, J.S.; methodology, J.S.; software, J.S. and H.S.; validation, J.S., H.S. and J.H.; investigation, J.S., H.S. and C.M.-M.; writing—original draft preparation, J.S., H.S. and J.H.; writing—review and editing, J.S., H.S., C.M.-M. and J.H.; visualization, C.M.-M. and J.S.; project administration, H.S.; funding acquisition, H.S. All authors have read and agreed to the published version of the manuscript.

Funding: This research received funding from Business Finland, Fortum Oyj, Helen Oy and Vantaan Energia Oy within the project EcoSMR Finnish Ecosystem for Small Modular Reactors, grant number 4410/31/2020.

Data Availability Statement: Not applicable.

Conflicts of Interest: The authors declare no conflict of interest.

Nomenclature

Abbreviations

BC	Baffle Cut
CAPEX	Capital expense
CR	Crossover Rate
CS	Cuckoo Search
CTL	Centerline Tube Limit
CV	Containment Vessel
DE	Differential Evolution
DH	District Heating
FOB	Free On-Board
HX	Heat Exchanger
NFE	Number of Function Evaluations
NP	Number of Parents (population size)
O and M	Operation and Maintenance
OTL	Outer Tube Limit
PWR	Pressurized Water Reactor
RPV	Reactor Pressure Vessel
SMR	Small Modular Reactor
SS	Sealing Strip
STHE	Shell-and-Tube Heat Exchanger
TCI	Total Capital Investment

Greek symbols

α	1. iteration loop damping factor [-] 2. scaling factor for Lévy flight step length [-]
β	Lévy exponent [-]
ε	1. effectiveness [-] 2. ratio of projected obstruction area to free-flow area without obstruction [-] 3. random number [-]
F	heat rate; thermal power [MW]
γ	intermittency factor [-]
μ	dynamic viscosity [Pa s]
ρ	density [kg/m ³]
θ	tube pitch angle [°]
ψ	void fraction [-]

Latin Symbols

a	annuity factor [-]
A	area [m ²]
c	specific cost [€/MWh]; [€/kW]; [€/kg]
c_p	specific heat [kJ/kgK]
C	cost [€]
C_f	Fanning coefficient of friction [-]
C^*	ratio of heat capacity rates
d	1. heat transfer tube diameter [m]; [mm] 2. variable index in a matrix of D decision variable values
D	1. diameter [m] 2. number of decision variables [-]
e^+	roughness Reynolds number
E	energy [MWh]
f_x	correction factors for shell-side heat transfer calculation [-]
f_D	Darcy friction factor [-]
F	mutation weight in differential evolution [-]

h	heat transfer coefficient [W/m ² K]
H	height [m]
k	thermal conductivity [W/mK]
K	loss coefficient [-]
l	characteristic length [-]
L	length [m]
m	mass [kg]
\dot{m}	mass flow rate [kg/s]
N_x	number of x [-]
NTU	number of transfer units (dimensionless conductance) [-]
Nu	Nusselt number [-]
p	pressure [bar]; [MPa]
p_a	switching probability: fraction of population subjected to Lévy flights [-]
\mathbf{p}	normal-distributed random variable vector [-]
P	tube pitch [m]; [mm]
Pr	Prandtl number [-]
\mathbf{q}	normal-distributed random variable vector [-]
Q	heat [MWh]
R''_{tf}	thermal resistance, fouling [m ² K/W]
Re	Reynolds number [-]
s	thickness [m]; [mm]
\mathbf{s}	Lévy-distributed step size vector [-]
S	spacing [m]
t	time [h]; [s]
T	temperature [°C]
\mathbf{u}	trial vector [-]
U	overall heat transfer coefficient [W/m ² K]
v	processing speed [m/min]
w	velocity [m/s]
\mathbf{x}	decision variable vector representing a candidate solution in population [-]
Subscripts	
bf	baffle plate
calc	calculation result in iterative solution
cav	reactor pool cavity
d	index for decision variable
excav	excavation
h	hydraulic
i	inside
in	inlet
man	manufacturing
mat	material
max	maximum
min	minimum
o	outside
out	outlet
pr	processing
Q	cross-flow zone in heat exchanger shell side
QE	last and first cross-flow zones in heat exchanger shell side
sh	shell
tb	heat transfer tube
tf	thermal, fouling
tgt	target value in iterative solution
w	1. wall 2. baffle window

Appendix A. Pressure Vessel Sizing

The shell-and-tube heat exchanger mechanical sizing (STHE) code is based on that developed earlier for conventional STHE exchangers [16] and condensers [17]; the full code is available in Supplementary Material S4.

Appendix A.1. Thickness of a Cylindrical Shell

The minimum acceptable shell thickness $s_{sh,min}$ of a cylindrical pressure vessel shell (the heat exchanger shell, or the cylindrical parts of the RPV or the CV) is the sum of required thickness $s_{s,0}$, corrosion allowance c_1 , and manufacturing tolerance c_2 ,

$$s_{sh,min} = s_{sh,min,0} + c_1 + c_2 \quad (A1)$$

where the required thickness $s_{s,min,0}$ is equal to the greatest of the results obtained from sizing a cylindrical pressure vessel body against elastic buckling, $s_{cyl,eb}$, non-elastic buckling, $s_{cyl,neb}$, and internal pressure, $s_{cyl,ip}$.

For elastic buckling, an explicit equation for the thickness is not stated in [31]; a maximum acceptable pressure $p_{max,eb}$ for a given thickness is defined instead,

$$p_{max,eb} = \frac{E_t}{n_{SF}} \left\{ \frac{2}{(N_{bw}^2 - 1) \left[1 + \left(\frac{N_{bw}}{C} \right)^2 \right]^2} \cdot \frac{s}{D_o} + \frac{2}{3(1 - \nu^2)} \left[N_{bw}^2 - 1 + \frac{2N_{bw}^2 - 1 - \nu}{1 + \left(\frac{N_{bw}}{C} \right)^2} \right] \left(\frac{s}{D_o} \right)^3 \right\}, \quad (A2)$$

where n_{SF} is a safety factor, $n_{SF} = 3$ with out-of-roundness of 0.015 or less, the auxiliary parameter C is obtained from

$$C = \frac{\pi D_o}{L}, \quad (A3)$$

and N_{bw} is the number of buckling waves. Equation (A2) is solved for all integer numbers $N_{bw} \in \{2, \dots, N_{bw,max}\}$, the smallest obtained pressure defining the $p_{max,eb}$. The upper limit $N_{bw,max}$ for the number of buckling waves is found by rounding up to the next integer the value $N_{bw,max}$ from

$$N_{bw,max} = 1.63 \sqrt{\frac{D_o}{L}} \sqrt{\frac{D_o}{s}}. \quad (A4)$$

Sizing against elastic buckling with the implicit Equation (A2) is performed by converting the sizing problem into a one-dimensional optimization problem to minimize the difference between the design pressure and the calculated pressure p_{calc} obtained from Equation (A2), where s_{eb} is the solution to

$$\min |p_{calc} - p_{des}| = f(s), \quad (A5)$$

applying Equation (A2) as the function f . The optimization is performed with Golden Section Search (GSS), as described in [59]. Two initial guesses, s_a and s_b , are chosen; one low and the other high enough to bracket the solution. These are then iteratively moved closer until $s_a - s_b \leq 0.01$ mm. From the dimensions, the total volume of material can be obtained, and, with a density of $r_{316L} = 7890$ kg/m³, the mass.

Against non-elastic buckling, the maximum pressure for wall thickness s is

$$p_{max,neb} = \frac{2\sigma}{n_{SF}} \frac{s}{D_o} \frac{1}{1 + 1.5e \left(1 - \frac{D_o}{5L} \right) \frac{D_o}{s}}, \quad (A6)$$

where a maximum acceptable shell out-of-roundness value of $e = 0.015$ is applied. The thickness is then obtained as with the elastic buckling by converting the problem to a one-dimensional optimization problem minimize the difference between design and calculation pressures, Equation (5), and applying Equation (A6) for the function f .

Against internal pressure p , the minimum wall thickness of a cylindrical vessel s_{ip} is

$$s_{ip} = \frac{D_o p}{\frac{2\sigma}{n_{SF}} - p}. \quad (A7)$$

Appendix A.2. Tubesheet Thickness

The thickness of the tubesheet s_{ts} is obtained from

$$s_{ts} = C D_o \sqrt{\frac{p_{\max} n_{SF}}{\sigma v}}, \quad (A8)$$

where p_{\max} is the greater of the hot and cold fluid design pressures; here, 1.0 MPa, C is a constant with a value of $C = 0.50$ for tube sheets welded from one side to the shell and exceeding a thickness of three shell thicknesses $3s_{sh}$, and v is a correction factor,

$$v = v_W v_H, \quad (A9)$$

where the weld strength correction v_W for austenitic stainless steel can be assumed as 1.0 when all welds are inspected, and v_H is the hole field correction,

$$v_H = \frac{P - d_o}{P} \quad (A10)$$

Appendix B. Heat Exchanger Material Costs

The heat exchanger material cost $C_{mat,HX}$ is obtained using the material volume, density, and specific costs. Table A1 lists the equations for the volumes of the main components, as well as the specific costs c .

Table A1. Material volumes and specific costs of different heat exchanger components.

Component x	Volume V_x [m ³]	Spec. Cost c_x [€/kg]
Shell	$V_{sh} = L_{tb,tot} \frac{\pi}{4} (D_{sh,o}^2 - D_{sh,i}^2)$ (A11)	6.09
Tubes	$V_{tb} = N_{tb} L_{tb,tot} \frac{\pi}{4} (d_o^2 - d_i^2)$ (A12)	29.0
Tubesheet	$V_{ts} = 2 \cdot s_{ts} \frac{\pi}{4} D_{ts}^2$ (A13)	8.11 ¹
Baffle plates	$V_{bfls} = N_{bf} V_{1bf}$ (A14)	7.66 ²
	$V_{1bf} = \frac{\pi}{4} D_{bf}^2 - \frac{D_{bf}^2}{8} (\alpha - \sin \alpha)$ (A15)	
Other	$V_{oth} = V_{rods} + V_{sps} + V_{ss}$ (A16)	6.09
	$V_{rods} = N_{rods} (L_{tb,tot} - 2 s_{ts}) \frac{\pi}{4} d_{rod}^2$ (A17)	
	$V_{sps} = N_{sps} (L_{tb,tot} - 2 s_{ts}) \frac{\pi}{4} (d_{sp,o}^2 - d_{sp,i}^2)$ (A18)	
	$V_{ss} = 2 \cdot N_{ss} (L_{tb,tot} - 2 s_{ts}) \cdot s_{ss} \cdot B_{ss}$ (A19)	
Scrap	V_{sc}	1.60

¹ estimated by assuming 45% scrap per circular disc area when cut from rectangular sheet. ² estimated by assuming 35% scrap per segmental baffle area cut from rectangular sheet.

Some amount of the material, purchased as tubes, pipe, plates, and rods, is also lost as scrap in processing; a value of $c_{sc} = 1.6$ €/kg is assumed for this. The baffle plate and tube sheet costs already account for the estimated amount of scrap from cutting discs or segmentally-cut baffle plates from rectangular plate. Additional scrap is also produced from drilling the holes in the tube sheet and baffle plates $V_{sc,h}$

$$V_{sc,h} = (N_{bf} N_{h,bf} s_{bf} + 2 \cdot N_{tb} s_{ts}) \frac{\pi}{4} d_{th}^2. \quad (A20)$$

Scrap is also produced when standard 6-m heat transfer tubes are cut to the specified length and drilling holes. This is accounted for by determining an effective tube price

$$c_{tb,eff} = c_{tb} + \frac{(c_{tb} - c_{sc}) \cdot \text{mod}(6.000; L_{tb,tot})}{6.000 - \text{mod}(6.000; L_{tb,tot})}, \quad (\text{A21})$$

with which the tube material cost is evaluated. With these parameters, the material cost is found using the components volumes, specific costs, and material density,

$$C_{mat,HX} = \sum_x c_x V_x \rho_{316L} - c_{sc} V_{sc,h} \rho_{316L}. \quad (\text{A22})$$

Appendix C. Heat Exchanger Processing Cost

The costs per operation include the sum of total costs of labour, machinery amortization, and consumables and utilities consumed; assembly considers labour only. Baffle drilling is assumed to take place by placing and aligning the baffles precisely on top of each other and fastening them tightly for drilling through multiple (but no more than five) plates at a time. It should be noted that the processing speed and cost estimates are highly uncertain and can vary greatly between the manufacturers, depending on the type of equipment used.

Table A2. Processing costs; baffle dimensions those depicted in Figure 6.

Process x	Processing Length L_x [m]	Speed v_x [$\frac{m}{min}$]	Spec. Cost $c_{t,x}$ [€/h]
Cutting baffles (bf) and sealing strips (ss)	$L_{cut} = N_{bf} L_{cut,1bf} + 2N_{ss}(2L_{ss} + 2W_{ss})$ (A23) $L_{cut,1bf} = \frac{2\pi - \alpha}{2} D_{bf} + 2\sqrt{H(D_{bf} - H)} + 2N_{ss}(2W_{ss} + s_{ss})$ (A24)	$v_{cut} = 0.5^*$	100
Beveling	$L_{bev} = L_{cut}$ (A25)	$v_{bev} = 1.5^*$	60
Drilling	$L_{dr} = N_{bf} N_{h,bf} s_{bf} + \text{ceil}\left(\frac{N_{bf}}{5}\right) (L_{lt} + L_{pt} + L_{ot})$, $L_{lt} = 3.0$ mm, drill head lead travel [32] $L_{pt} = 5.0$ mm, drill head pre-travel [32] $L_{ot} = 5.0$ mm, drill head over-travel [32] (A26)	$v_{dr} = \frac{\ln d_o}{18.2} + \frac{1}{83}^{\S}$	80
Bundle assembly	n/a	n/a	50

* estimate based on [32] with the assumption of stainless steel processing speed being 50% of that of carbon steel.
 \S [d_o]=mm; yields result as m/min. The function is a curve fit on a drill bit of manufacturer's recommended feed rate and RPM with carbide tips for different hole diameters on a stainless steel plate.

Table A3. Processing costs; set-up and loading times for different operations.

Process x	Time to Move, Load and Set Up $t_{su,x}$ [min]	Specific Cost $c_{t,x}$ [€/h]
Cutting baffles and sealing strips	10 min per plate + 5 min	100
Beveling	10 min per plate + 5 min	60
Drilling	5 min per 1 plate + 10 min per 5 plates	80
Bundle assembly	30 min general setup 5 s for each tube through 1 hole in 1 baffle 2 min per sealing strip per baffle 20 min per baffle for tie rods and spacers	50

Appendix D. Modified Cuckoo Search CS3/Rand/1/Bin

Algorithm A1. Pseudo-code for CS3/rand/1/bin to maximize function $f(x)$, $x = (x_1, \dots, x_D)^T$. MATLAB code is available from Supplementary Material S3.

```

begin
Randomly initialize a population of  $NP$  cuckoos (eggs)  $x_i$ ,  $i = 1, 2, \dots, NP$ 
for all  $x_i$  do
    Evaluate objective function to find  $F_i = f(x_i)$ 
end for
while  $NFE < NFE_{max}$  do
    for all  $x_i$  do
        Create a trial egg  $u_i^G$  by Equation (29)
        Find objective function value  $F_{u(i)^G}$ 
        if  $(F_{u(i)^G} > F_i^G)$ 
             $x_i^{G+1} \leftarrow u_i^G$ 
             $F_i^{G+1} \leftarrow F_{u(i)^G}$ 
        end if
    end for
    Rank all solutions according to their objective function values  $F$ 
    for worst  $(p_a \cdot NP)$  solutions do
        Create a trial egg  $u_i^G$  by taking a Lévy flight from  $x_i^G$ , Equation (30)
        Find objective function value  $F_{u(i)^G} = f(u_i^G)$ 
         $x_i^{G+1} \leftarrow u_i^G$ 
         $F_i^{G+1} \leftarrow F_{u(i)^G}$ 
    end for
end while
end

```

References

1. Statistics Finland. Energy 2021 Table Service. Available online: https://pxhoepa2.stat.fi/sahkoiset_julkaisut/energia2021/html/engl0002.htm (accessed on 18 January 2023).
2. Finnish Energy Association. *District Heating in Finland 2021*; Finnish Energy Association: Helsinki, Finland, 2022; Available online: https://energia.fi/files/5695/District_heating_2021_v2.pdf (accessed on 18 January 2023).
3. Finnish Energy Association. *Finnish Energy Attitudes 2021*; Finnish Energy Association: Helsinki, Finland, 2022; Available online: https://energia.fi/files/7560/Finnish_Energy_Attitudes_2022.pdf (accessed on 30 January 2023).
4. Sandström, S. (Ed.) *Operating Experience at the Ågesta Nuclear Power Station*; Aktiebolaget Atomenergi: Stockholm, Sweden, 1966.
5. International Atomic Energy Agency (IAEA). *Status of Non-Electric Nuclear Heat Applications: Technology and Safety*; IAEA-TECDOC-1184; IAEA: Vienna, Austria, 2000; ISSN 1011-4289.
6. International Atomic Energy Agency (IAEA). *Advances in Small Modular Reactor Technology Developments a Supplement to: IAEA Advanced Reactors Information System (ARIS)*; IAEA: Vienna, Austria, 2022; Available online: https://aris.iaea.org/Publications/SMR_booklet_2022.pdf (accessed on 5 January 2023).
7. Värri, K.; Syri, S. The Possible Role of Modular Nuclear Reactors in District Heating: Case Helsinki Region. *Energies* **2019**, *12*, 2195. [[CrossRef](#)]
8. Podest, M. Reactors for low-temperature nuclear heat supply. *Nucl. Eng. Des.* **1988**, *109*, 115–121. [[CrossRef](#)]
9. Nilsson, L.; Hannus, M. SECURE nuclear district heating plant. *Nucl. Technol.* **1978**, *38*, 225–234. [[CrossRef](#)]
10. Wenxiang, Z.; Dazhong, W. NHR-200 nuclear energy system and its possible applications. *Prog. Nucl. Energy* **1995**, *29*, 193–200. [[CrossRef](#)]
11. Dazhong, W.; Dafang, Z.; Duo, D.; Zuying, G.; Huaixuan, L.; Jiagui, L.; Qingshan, S. Experimental study and operation experiences of the 5 MW nuclear heating reactor. *Nucl. Eng. Des.* **1993**, *143*, 9–18. [[CrossRef](#)]
12. Teräsvirta, A.; Syri, S.; Hiltunen, P. Small Nuclear Reactor—Nordic District Heating Case Study. *Energies* **2020**, *13*, 3782. [[CrossRef](#)]
13. Truong, T.; Suikkanen, H.; Hyvärinen, J. Reactor core conceptual design for a scalable heating experimental reactor, LUTHER. *J. Nucl. Eng.* **2021**, *2*, 207–214. [[CrossRef](#)]
14. Leppänen, J.; Valtavirta, V.; Rintala, A.; Hovi, V.; Tuominen, R.; Peltonen, J.; Hirvensalo, M.; Dorval, E.; Lauranto, U.; Komu, R. Current Status and On-Going Development of VTT's Kraken Core Physics Computational Framework. *Energies* **2022**, *15*, 876. [[CrossRef](#)]
15. Leppänen, J.; Hillberg, S.; Hovi, V.; Komu, R.; Kurki, J.; Lauranto, U.; Oinonen, A.; Peltonen, J.; Rintala, A.; Tulkki, V.; et al. A Finnish District Heating Reactor: General overview. In Proceedings of the ICONE-28, Virtual Conference, 4–6 August 2021.

16. Saari, J.; Garcia Perez, M.; Neto, M.; Cardoso, M.; Vakkilainen, E.; Kaikko, J. Shell-and-tube heat exchanger optimization—Impact of problem formulation and cost function. In Proceedings of the 14th International Conference on Heat Transfer, Fluid Mechanics, and Thermodynamics (HEFAT 2019), Wicklow, Ireland, 22–24 July 2019; pp. 1350–1356.
17. Saari, J.; Martinez, C.M.; Kaikko, J.; Sermyagina, E.; Mankonen, A.; Vakkilainen, E. Techno-economic optimization of a district heat condenser in a small cogeneration plant with a novel greedy cuckoo search. *Energy* **2022**, *239*, 122622. [[CrossRef](#)]
18. Sörensen, K. Metaheuristics—The metaphor exposed. *Int. Trans. Oper. Res.* **2013**, *22*, 3–18. [[CrossRef](#)]
19. Lones, M.A. Mitigating metaphors: A comprehensible guide to recent nature-inspired algorithms. *SN Comput. Sci.* **2020**, *1*, 49. [[CrossRef](#)]
20. Afanasyeva, S.; Saari, J.; Kukkonen, S.; Partanen, J.; Pyrhönen, O. Optimization of wind farm design taking into account uncertainty in input parameters. In Proceedings of the European Wind Energy Conference & Exhibition, 2013, EWEC, Vienna, Austria, 4–7 February 2013; pp. 1808–1810.
21. Neto, M.; Saari, J.; Vakkilainen, E.; Oliveira, É.; Cardoso, M. A superstructure-based methodology for simultaneously sizing and arranging additional evaporator bodies in multiple-effect evaporator plants. *JFor-J. Sci. Technol. Prod. Proc.* **2020**, *7*, 36–47.
22. Afanasyeva, S.; Saari, J.; Pyrhönen, O.; Partanen, J. Cuckoo search for wind farm optimization with auxiliary infrastructure. *Wind Energy* **2018**, *21*, 855–875. [[CrossRef](#)]
23. VALOR Partners Oy. *Demand Flexibility in District Heating*; Finnish Energy Association: Helsinki, Finland, 2015; p. 12. Available online: http://energia.fi/files/439/Kaukolammon_kysyntajousto_loppuraportti_VALOR.pdf (accessed on 12 November 2022). (In Finnish)
24. Jylhä, K.; Kalamees, T.; Tietäväinen, H.; Ruosteenoja, K.; Jokisalo, J.; Hyvönen, R.; Ilomets, S.; Saku, S.; Huttila, A. *Test Reference Year 2012 for Building Energy Demand and Impacts of Climate Change*; Finnish Meteorological Institute: Helsinki, Finland, 2011; p. 84. (In Finnish)
25. Koskelainen, L.; Saarela, R.; Sipilä, K. *Handbook of District Heating (in Finnish: Kaukolämmön käsikirja)*; Finnish Energy Association: Helsinki, Finland, 2003; p. 336.
26. Viander, T. Optimization of District Heating Network Usage. Master’s Thesis, Lappeenranta University of Technology, Lappeenranta, Finland, 2014. (In Finnish).
27. Sinnott, R.K. *Coulson & Richardson’s Chemical Engineering Design Vol 6*, 4th ed.; Butterworth-Heinemann: Oxford, UK, 2005.
28. Lindroos, T.J.; Pursiheimo, E.; Sahlberg, V.; Tulkki, V. A techno-economic assessment of NuScale and DHR-400 reactors in a district heating and cooling grid. *Energy Sources Part B Econ. Plan. Policy* **2019**, *14*, 13–24. [[CrossRef](#)]
29. Saari, J.; Afanasyeva, S.; Vakkilainen, E.; Kaikko, J. Heat transfer model and optimization of a shell-and-tube district heat condenser. In Proceedings of the 27th International Conference on Efficiency, Cost, Optimization, Simulation, and Environmental Impact of Energy Systems (ECOS 2014), Turku, Finland, 15–19 June 2014.
30. *SFS-EN 13445-3; Unfired Pressure Vessels*. CRC Press: Boca Raton, FL, USA, 2002. (In Finnish)
31. British Stainless Steel Association. *Elevated Temperature Physical Properties of Stainless Steels*; British Stainless Steel Association: Sheffield, UK. Available online: https://bssa.org.uk/bssa_articles/elevated-temperature-physical-properties-of-stainless-steels/ (accessed on 12 December 2022).
32. Caputo, A.C.; Pelagagge, P.M.; Salini, P. Manufacturing cost model for heat exchangers optimization. *Appl. Therm. Eng.* **2016**, *94*, 513–533. [[CrossRef](#)]
33. Mauri, M. Economics of Nuclear Power Plants: Bottom-Up Cost Estimation Model for Small Modular Reactors. Master’s Thesis, Politecnico di Milano, Milano, Italy, 2021.
34. Paparusso, L. *Bottom-Up Cost Estimation of Small Modular PWR*; Politecnico di Milano: Milano, Italy, 2012.
35. Statistics Finland. *Producer Price Indices 2021*. Available online: https://www.stat.fi/til/thi/2021/index_en.html (accessed on 26 December 2022).
36. The Economic Modeling Working Group of the Generation IV International Forum. *Cost Estimating Guidelines for Generation IV Nuclear Energy Systems*; Revision 4.2; OECD Nuclear Energy Agency for the Generation IV International Forum: Paris, France, 2007; Available online: https://www.gen-4.org/gif/upload/docs/application/pdf/2013-09/emwg_guidelines.pdf (accessed on 23 December 2022).
37. Statistics Finland. Building Cost Index: Building Costs Rose by 0.6 Per Cent in January Year-on-Year. Available online: https://www.stat.fi/til/rki/2021/01/rki_2021_01_2021-02-15_en.pdf (accessed on 23 December 2022).
38. Heat Exchange Institute. *Standards for Closed Feedwater Heaters*, 7th ed.; Heat Exchange Institute: Cleveland, OH, USA, 2010.
39. Álvarez-Fernández, M.; del Portillo-Valdés, L.; Alonso-Tristán, C. Thermal analysis of closed feedwater heaters in nuclear power plants. *Appl. Therm. Eng.* **2014**, *68*, 45–58. [[CrossRef](#)]
40. Gnielinski, V. New equations for heat and mass transfer in turbulent flow in pipe and channel flow. *Int. Chem. Eng.* **1976**, *16*, 359–368.
41. Bhatti, M.S.; Shah, R.K. Turbulent and transition flow convective heat transfer in ducts. In *Handbook of Single-Phase Convective Heat Transfer*, 1st ed.; Kakaç, S., Shah, R.K., Aung, W., Eds.; Wiley-Interscience: Hoboken, NJ, USA, 1987; Volume 3, pp. 4.1–4.163.
42. Petukhov, B.S.; Popov, V.N. Theoretical calculation of heat exchange and frictional resistance in turbulent flow in tubes of an incompressible fluid with thermophysical properties. *High-Temp. Thermophys.* **1963**, *1*, 85–101. (In Russian)
43. Shah, R.K.; Sekulic, D.P. *Fundamentals of Heat Exchanger Design*; John Wiley & Sons: Hoboken, NJ, USA, 2003; p. 482.
44. Rotta, J.C. Turbulent Shear Flows. In *Turbulent Flows*; Rotta, J.C., Ed.; Verlag Teubner: Stuttgart, Germany, 1972; pp. 127–186. (In German)

45. Gnielinski, V. A new calculation method for heat transfer in the transition regime between laminar and turbulent pipe flow. *Res. Eng.* **1995**, *61*, 240–248. (In German) [[CrossRef](#)]
46. Gnielinski, V. Heat Transfer in Pipe Flow. In *VDI Heat Atlas*, 2nd ed.; Springer: Berlin/Heidelberg, Germany, 2010; pp. 693–699.
47. Norris, R.H. *Some Simple Approximate Heat-Transfer Correlations for Turbulent Flow in Ducts with Rough Surfaces*; General Electric Company Corporate Research and Development: Niskayuna, NY, USA, 1970.
48. Kays, W.; Crawford, M.; Weigand, B. *Convective Heat and Mass Transfer*, 4th ed.; McGraw-Hill: New York, NY, USA, 2004.
49. Che, N.H. An explicit equation for friction factor in pipe. *Ind. Eng. Chem. Fund.* **1979**, *18*, 296–297.
50. Gaddis, E.S.; Gnielinski, V. Shell-Side Heat Transfer in Baffled Shell-and-Tube Heat Exchangers. In *VDI Heat Atlas*, 2nd ed.; Springer: Berlin/Heidelberg, Germany, 2010; pp. 731–741.
51. Kast, W.; Nirschl, H. Pressure Drop in Flow Through Pipes of Changing Cross-section. In *VDI Heat Atlas*, 2nd ed.; Springer: Berlin/Heidelberg, Germany, 2010; pp. 1065–1075.
52. Gaddis, E.S. Pressure Drop in the Outer Shell of Heat Exchangers. In *VDI Heat Atlas*, 2nd ed.; Springer: Berlin/Heidelberg, Germany, 2010; pp. 1092–1105.
53. Todreas, N.E.; Kazimi, M.S. *Nuclear Systems—Volume 1—Thermal Hydraulic Fundamentals*, 2nd ed.; CRC Press, Taylor & Francis Group: Boca Raton, FL, USA, 2012; pp. 464–534.
54. Westinghouse AP1000 Design Control Document Rev. 19—Tier 2 Chapter 4—Reactor. Available online: <https://www.nrc.gov/docs/ML1117/ML11171A500.html> (accessed on 17 January 2023).
55. Yang, X.; Deb, S. Cuckoo search via Lévy flights. In Proceedings of the World Congress on Nature & Biologically Inspired Computing, Coimbatore, India, 9–11 December 2009.
56. Yang, X. *Nature-Inspired Optimization Algorithms*; Elsevier: Waltham, MA, USA, 2014.
57. Price, K.; Storn, R.M.; Lampinen, J. *Differential Evolution: A Practical Approach to Global Optimization*, 1st ed.; Springer: Heidelberg, Germany, 2006.
58. Mantegna, R.N. Fast, accurate algorithm for numerical simulation of Lévy stable stochastic processes. *Phys. Rev. E* **1994**, *49*, 4677–4689. [[CrossRef](#)] [[PubMed](#)]
59. Rao, S. *Optimization: Theory and Applications*; Wiley Cop.: New Delhi, India, 1979.

Disclaimer/Publisher’s Note: The statements, opinions and data contained in all publications are solely those of the individual author(s) and contributor(s) and not of MDPI and/or the editor(s). MDPI and/or the editor(s) disclaim responsibility for any injury to people or property resulting from any ideas, methods, instructions or products referred to in the content.